This article has been accepted for publication in a future issue of this journal, but has not been fully edited. Content may change prior to final publication. Citation information: DOI 10.1109/TIE.2019.2899546, IEEE Transactions on Industrial Electronics

Fault Ride-Through Strategy for Two-Stage GPV System Enabling Load Compensation Capabilities Using EKF Algorithm

Vedantham Lakshmi Srinivas, *Member, IEEE,* Bhim Singh, *Fellow, IEEE* and Sukumar Mishra, *Senior Member, IEEE*

Abstract: This paper proposes an extended Kalman filter (EKF) based control strategy for fault ride-through operation in two-stage grid-connected photovoltaic (GPV) system. Unlike the conventional controllers for ride-through operation, the proposed strategy does not compromise with power quality improvement features in the system while enabling ride-through operation. The controller accounts for nonlinear loads in the system, grid harmonic-currents elimination and grid-currents balancing even during the harmonic/distorted grid voltages. The IEEE standard-1547.4 compels the distributed resource to ride-through during voltage disturbances caused by faults. For the ride-through operation, a limit is imposed on PV active power injection to prevent inverter over-currents and DC-link energy aggregation, which reduces the lifetime of DC-link capacitor. The reactive power is fed to the grid, as per the depth in voltage-sag. The de-rated PV array power is supplied in cases where the inverter cannot handle the utmost PV-power. The power quality improvement is ensured using EKF state estimator, which precisely estimates the fundamental load currents. In distribution network with modern nonlinear loads, especially at far radial ends, the grid voltages are prone to huge diversions and the proposed controller provides a possible solution to maintain active/reactive power support and maintain power quality in the network. The effectiveness of the strategy is demonstrated through simulations and experiments. Under all disturbances, the harmonic content in grid currents is observed within limits, in accordance with the IEEE standard-519.

Keywords: Distributed generation, EKF, Total harmonic distortion (THD), Phase locked loop, PWM.

I. INTRODUCTION

WITH the emphasis on clean power generation, the renewable energy based distributed generation systems have received great attention. Accounting to the recent developments in photovoltaic technology, the solar photovoltaic (PV) based renewable power generation has experienced a swift growth among the commercial and residential sectors [1]. However, increased dissemination of solar PV power generation into the traditional grid, has led to various power quality problems, especially in distribution networks where a significant portion of renewable energy sources are connected [2]. The advent of different power electronic loads further deteriorated the power quality in the network. Various solutions are proposed in the literature addressing the power quality issues without affecting the load profile [2]-[3]. There is a long tradition of using linear controllers for power quality improvement in grid-interfaced systems however they have their own limitations [4]. Moreover, these control schemes [4] necessitate phase locked loops (PLLs), which increases the system complexity in practical implementation and leads to mal-operation under distorted grid voltages. Recently, the power quality improvement in the distribution grid using nonlinear modal predictive controller (MPC), is contemplated by the authors in [5], however, its performance under nonlinear loads, is not investigated. To improve power factor and to minimize line current harmonics, modal reference adaptive control (MRAC) is introduced in [6]. However, it requires knowledge of reference system a priori. These control strategies [3]-[6] focus on improving the power quality in distribution network, with active/ reactive power injection to the grid. Their operation under gird-side faults, voltage unbalances and voltage harmonic distortions, is not analyzed.

On the other hand, there are control strategies for grid interfaced inverters for ride through operation during balanced/unbalanced voltage sag faults, without focusing on the power quality improvement in the distribution grid [7]-[14]. The researchers have achieved the ride-through operation by injecting reactive power into the grid. During the unbalance in distribution grid voltages, the regulation of grid current becomes challenging. The control algorithms are contemplated to overcome this issue, either by balancing the grid currents or by minimizing the active power fluctuations. For instance, the authors in [7] have developed a stationary frame PQ controller to minimize the ripple content in active power through a gain parameter. A synchronous frame current regulator is contemplated in [8]-[9] for power control during unbalanced grid voltages. The functionality of unbalanced voltage compensation using DG inverters is reported in [10]-[13], which are based on symmetric components. In these control strategies, the DG inverters are controlled either through positive sequence active powers or positive sequence reactive powers [11]-[12] or both positive sequence active and reactive powers [10]-[13] for compensating the unbalanced voltages. The studies have also been made for ride-through operation during unbalanced voltage sags with controllable active/reactive power oscillations [15]-[18]. These strategies [7]-[18] depict different control approaches for ride-through operation in grid-interfaced distributed generation systems during grid voltage balanced/unbalanced sags. However, a) they fail to achieve the power quality improvement in distribution network through grid current harmonic compensation, b) they do not address the harmonic/distorted grid voltages caused at far radial ends in the distribution network, and c) they fail to address the dynamics of renewable

This article has been accepted for publication in a future issue of this journal, but has not been fully edited. Content may change prior to final publication. Citation information: DOI 10.1109/TIE.2019.2899546, IEEE Transactions on Industrial Electronics

energy resource (such as photovoltaic or wind) and the control of DC link voltage. The dynamics in PV arrays, DC-DC power conditioning stage and the DC-link capacitor, impact the operation of overall system, especially during the fault ride through analysis and consequently, the task becomes challenging. The control strategies that consider dynamics of photovoltaic power plants are reported in [19]-[23]. The controller [19] uses multiple proportional resonant (PR) controllers to achieve individual phase current compensation. The system performance with PR controllers, is degraded under variation of the system frequency as it provides infinite gain at the selected harmonic frequencies. The non-ideal implementation of infinite gains could cause series of instability issues for practical grid interfaced DG systems [24]. Besides this, these strategies [19]-[23] do not contribute for power quality improvement during nonlinear loads and harmonic voltages in the system. Moreover, the zero-sequence and negative-sequence powers are produced by unbalanced currents with unbalanced voltages, which badly affect different commercial loads and industrial loads connected at the higher end of the distribution system such as three-phase motor loads/ high power loads. The ride through operation of grid interfaced PV systems under low voltage sags, which ensures the different power-quality functionalities of harmonic current mitigation, power factor correction, balancing of grid currents, reliable operation during abnormal/harmonic grid voltages caused in distribution system, is seldom reported in literature.

In this paper, the EKF scheme based double-stage grid-interfaced solar PV system is proposed, to accomplish manifold objectives. Firstly, the ride-through operation of grid-interfaced double-stage solar PV system is evaluated under balanced/ unbalanced grid-side faults. During the grid faults, the PV inverter facilitates the quick detection and reacts accordingly to minimize the adverse effects on the inverter and grid-side equipment, to comply with IEEE Std. 1547.4. The system facilitates active and reactive power injection during the voltage-sag faults, so that the PV systems remain operational under such conditions without causing further instabilities due to loss of PV generation. Moreover, the proposed system is able to withstand the grid side harmonic/distorted voltages by supplying smooth and balanced sinusoidal grid currents. Contrary to many algorithms on ride through operation, the proposed control strategy is able to account for the nonlinear PCC loads in the distribution system, and compensates for the harmonic currents injected into the grid, even during the faults and harmonic voltage distortions. In this way, it satisfies the IEEE standard-519. The sinusoidal and balanced grid currents under all disturbances are ensured by incorporating a new way for extraction of unit-templates of grid voltages. This nullifies the negative sequence and zero sequence power injections into the grid during the grid voltage unbalances, thereby, the effect of sequence powers on industrial/commercial loads, is nullified. Besides this, a nonlinear Kalman filter is contemplated here. EKF is a mathematical method, which operates through prediction and correction mechanism, and it estimates the fundamental of the load current. It offers considerably better steady-state and dynamic performances, over the linear controllers [25]-[26], under system perturbations. It is a statistical technique and does not necessitate any dq-transformations, which are prone to errors if the synchronous frame identification is inaccurate, nor does it necessitates phase locked-loops. Its recursive structure allows real-time execution without storing observations or past estimates. The main contributions of the present work can be identified as follows.

- The fault ride through control strategy is presented for two-stage grid-interfaced solar PV system, that can handle harmonic/distorted grid voltages, caused at far radial ends in the distribution network, and still supply balanced and sinusoidal grid currents with THD with the limits depicted by IEEE Std. 519, despite severe voltage-sag faults.
- Contrary to several control strategies on ride-through operation, this control strategy accounts for nonlinear loads in the system, and compensates for unbalanced/harmonic loads during the voltage-sag faults and harmonic voltages.
- EKF control estimates the fundamental load currents, without the prior knowledge of amplitude, phase and behavior of the disturbances present in the load currents. The superior steady-state and dynamic performances of EKF based strategy over linear controllers are established.

The system is carefully evaluated through simulations and experiments. A prototype of two-stage grid interfaced PV system is developed in the laboratory and proposed control scheme is realized using DSP-dSPACE-1202 microlab-box controller. Experimental results validate the steady-state and dynamic performances of the system under different test conditions.

II. System Configuration

Fig. 1 shows the configuration of a double stage grid interfaced solar photovoltaic system with local loads connected at PCC (Point of Common Coupling). The system includes a PV array, three-phase voltage source inverter (VSI), the boost converter, interfacing inductors, DC link capacitor, ripple filter and the linear/nonlinear loads. The modeling methodology for PV array is reported in the literature [27]. A two-stage system is considered here, where the DC-DC boost converter ensures the maximum power extraction from the PV array, using incremental-conductance (InC) [28] based maximum power extraction technique, due the advantages it offers [28], in spite of a few demerits [28]. In InC algorithm, the direction of perturbation to reach maximum power point is decided by the difference between the incremental conductance and the

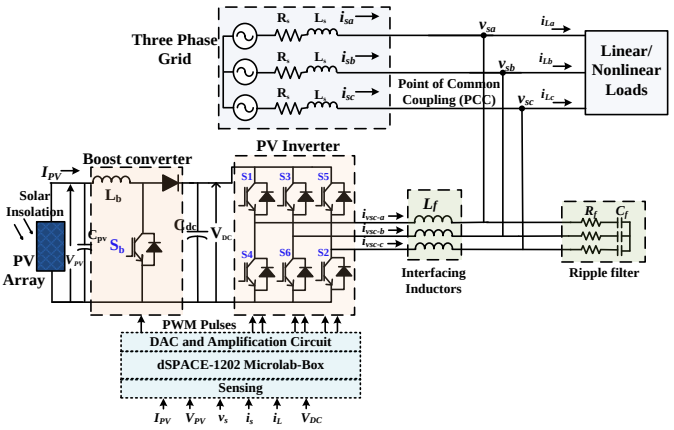

Fig. 1 Configuration of two-stage grid interfaced PV system

This article has been accepted for publication in a future issue of this journal, but has not been fully edited. Content may change prior to final publication. Citation information: DOI 10.1109/TIE.2019.2899546, IEEE Transactions on Industrial Electronics

conductance offered by the PV array. However, under severe grid side faults, the PV array is made to operate under non-MPPT mode, as the PV inverter cannot handle the maximum PV power. The ripples in the grid currents are eliminated using interfacing inductors and the VSI switching noises are absorbed by the ripple filter. The design and modelling procedure of the system, is as presented in [2]. The details of system parameters are reported in Appendix.

III. CONTROL APPROACH

The systematic control for the grid interfaced power converter and the boost converter, are described here. The necessary inputs to the PV inverter, are grid currents (i_{sa}, i_{sb}, i_{sc}), load currents(i_{La}, i_{Lb}, i_{Lc}), PCC voltages (v_{sa}, v_{sb}, v_{sc}) and the DC link voltage (V_{DC}); whereas the boost converter controller primarily requires PV-array voltage (V_{PV}) and current (I_{PV}) as its inputs. The reference grid currents are evaluated using the control scheme and the hysteresis controller is used to ensure that the sensed grid currents follow the reference grid currents. The overall control schematic for PV inverter, is depicted in Fig. 2. The different objectives of the control, are demonstrated by division of control into five modules namely, (i) load currents processing through EKF scheme, (ii) assigning the load current weights, (iii) evaluation of loss component and the PV feed forward component, (iv) fault ride through control, and (v) generation of inverter gating pulses. These are explained as follows.

A. EKF Scheme for Load Currents Processing

The EKF scheme for estimation of fundamental components of load current, is described here. The KF is mathematical procedure, which operates through prediction and correction mechanism. It is a recursive structure allows its real-time execution without storing observations or past estimates. It provides information about the quality of the estimation by providing, in addition to the best estimate, the variance of the estimation error.The KF has the ability to correct itself and takes the advantage of corrections between unknown dynamics and update itself. In essence, the KF algorithm predicts a new state from its previous estimation by adding a correction term proportional to predicted error. In this way, this error is statistically minimized.

Initially, the load current, is expressed as,

$$i_{La} = \sum_n I_{Lan} \cos(\omega_n t + \phi_n) \tag{1}$$

where, I_{pn}, ϕ_n, ω_n are amplitude, phase and frequency of the n[th] harmonic component. The load current at k[th] sampling instant (y_k), is expressed as,

$$y_k = I_{La1} \cos(k\omega_1 T_s + \phi_1) + \varepsilon_k \tag{2}$$

where, 'T_s' is the sampling time and ε_k is Gaussian noise with zero mean and variance σ_v^2. The expression (2) is stated in terms of estimated fundamental load current ($\hat{y}_k$) as,

$$y_k = \hat{y}_k + \varepsilon_k \tag{3}$$

After considering three consecutive samples of load currents at sampling time T_s, the single sinusoid, '$\hat{y}_k$' satisfies the following relationship,

$$\hat{y}_k - 2\cos k\omega T_s \hat{y}_{k-1} + \hat{y}_{k-2} = 0 \tag{4}$$

The estimated state-space vector at (k-1)[th] instant is defined as,

$$\hat{x}_{k-1|k-1} = \begin{bmatrix} 2\cos(k-1)\omega T_s & \hat{y}_{k-1} & \hat{y}_{k-2} \end{bmatrix}^T \tag{5}$$

The corresponding signal at k[th] instant can be identified as,

$$\hat{x}_{k|k-1} = \begin{bmatrix} 1 & 0 & 0 \\ 0 & 2\cos k\omega T_s & -1 \\ 0 & 1 & 0 \end{bmatrix} \hat{x}_{k-1|k-1} \tag{6}$$

The '$\hat{x}_{k-1|k-1}$' represents the estimated state variable at (k-1)[th] instant with given values at (k-1)[th] instant; and '$\hat{x}_{k|k-1}$' represents the estimated state variable at k[th] instant with given values at (k-1)[th] instant. Thus, from (4)-(6), (3) can be expressed as,

$$y_k = \begin{bmatrix} 0 & 2\cos k\omega T_s & -1 \end{bmatrix} \hat{x}_{k|k-1} + \varepsilon_k \tag{7}$$

Nonlinear equations (6)-(7), are formulated as,

$$\hat{x}_{k|k-1} = f(\hat{x}_{k-1|k-1}) \text{ and } y_k = g(\hat{x}_{k|k-1}) + \varepsilon_k \tag{8}$$

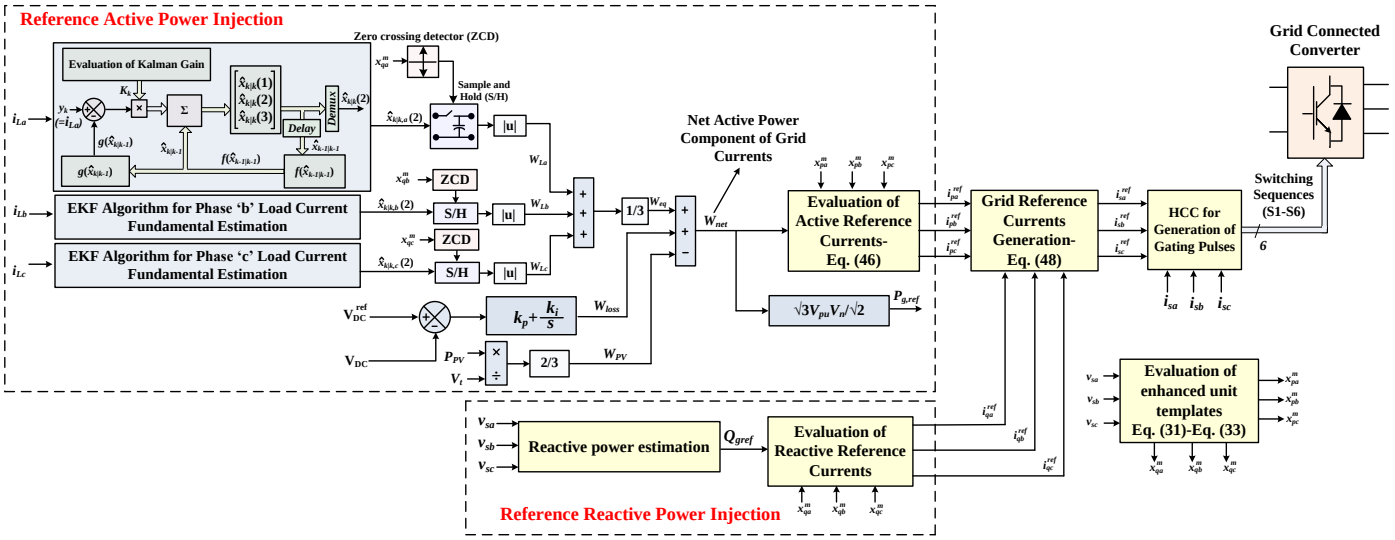

Fig. 2 Control schematic for generation of PV inverter gating pulses

This article has been accepted for publication in a future issue of this journal, but has not been fully edited. Content may change prior to final publication. Citation information: DOI 10.1109/TIE.2019.2899546, IEEE Transactions on Industrial Electronics

where,

$$f(\hat{x}_{k-1|k-1}) = \begin{bmatrix} 1 & 0 & 0 \\ 0 & 2\cos k\omega T_s & -1 \\ 0 & 1 & 0 \end{bmatrix} \hat{x}_{k-1|k-1} \quad (9)$$

$$\hat{y}_k = g(\hat{x}_{k|k-1}) = \begin{bmatrix} 0 & 2\cos k\omega T_s & -1 \end{bmatrix} \hat{x}_{k|k-1} \quad (10)$$

The nonlinear recursive filter is applied to estimate the magnitude of the signal and its frequency even under presence of the noise, by linearizing the system (8)-(10) as,

$$\hat{x}_{k|k-1} = f(\hat{x}_{k-1|k-1}) \quad (11)$$

$$\hat{x}_{k|k} = \hat{x}_{k|k-1} + K_k(y_k - g(\hat{x}_{k|k-1})) \quad (12)$$

Thus the estimated state vector $\hat{x}_{k|k}$ from (12), estimated for kth instant, is applied to system. The Kalman gain (K_k) in (12) is evaluated as,

$$K_k = \hat{P}_{k|k-1} \left.\frac{\partial g^T}{\partial \hat{x}}\right|_{(k|k-1)} \left[\left.\frac{\partial g}{\partial \hat{x}}\right|_{(k|k-1)} \hat{P}_{k|k-1} \left.\frac{\partial g^T}{\partial \hat{x}}\right|_{(k|k-1)} + R_o \right]^{-1} \quad (13)$$

The error covariance vector ($\hat{P}_{k|k-1}$) is evaluated and updated as follows.

$$\hat{P}_{k|k-1} = \left.\frac{\partial f}{\partial \hat{x}}\right|_{k|k-1} \hat{P}_{k-1|k-1} \left.\frac{\partial f^T}{\partial \hat{x}}\right|_{k|k-1} + Q_o \quad (14)$$

$$\hat{P}_{k|k} = \hat{P}_{k|k-1} - K_k \left.\frac{\partial g}{\partial \hat{x}}\right|_{k|k-1} \hat{P}_{k|k-1} \quad (15)$$

$$\left.\frac{\partial f}{\partial \hat{x}}\right|_{x_k = \hat{x}_{k|k-1}} = \begin{bmatrix} 1 & 0 & 0 \\ \hat{x}_{k|k-1}(2) & \hat{x}_{k|k-1}(1) & -1 \\ 0 & 1 & 0 \end{bmatrix} \quad (16)$$

$$\left.\frac{\partial g}{\partial \hat{x}}\right|_{x_k = \hat{x}_{k|k-1}} = \begin{bmatrix} \hat{x}_{k|k-1}(2) & \hat{x}_{k|k-1}(1) & -1 \end{bmatrix} \quad (17)$$

Here, Q_o and R_o are the covariance matrices associated with the process noise (w_k) and the measurement noise (i.e. ε_k). The R_o and Q_o for EKF, are typically initialized as 10^{-4} and $10^{-4}I_{3\times3}$, respectively [29].

In (13), however, $R_k = R_o e^{\|y_k - g(\hat{x}_{k|k-1})\|^2}$ is considered instead of R_o, by assigning the exponential term of error between sensed load current and estimated fundamental load component, to the error covariance term. If the error between sensed and estimated components, is high, then, the exponential factor increases faster, which increases the error covariance term and mitigation of error is achieved. Thus, robust performance of the EKF, is achieved by incorporating exponential term, under high disturbances in the load current.

The state prediction is used to compute the value at time point *k* based on the estimated value at time point *k-1*. If current dynamics is largely varied at time point *k-1*, the estimator is not capable to follow the situation and provides appropriate weighting. As a result, it is not capable to predict a value that is close to the real value at time point *k*. Nevertheless, the algorithm still outputs the appropriate value, because the innovation vector ($y_k - g(\hat{x}_{k|k-1})$) swiftly changes under such conditions, amplifying the Kalman gain. The estimated three phases fundamental load currents ($\hat{x}_{k|k,a}(2), \hat{x}_{k|k,b}(2), \hat{x}_{k|k,c}(2)$) are thus obtained and processed further to generate the switching pulses of VSI. The block diagram representing the process, is shown in Fig. 3.

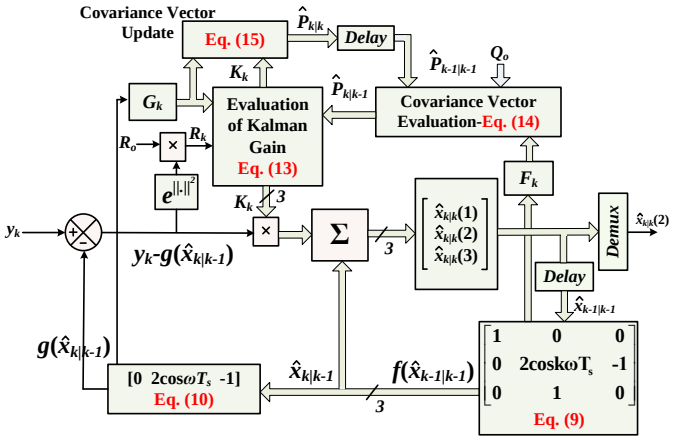

Fig. 3 Implementation of EKF algorithm

As depicted earlier, the estimated state vector $\hat{x}_{k|k}$ from (12), is estimated for kth instant, is the output of the EKF control. Its deviation from the actual state vector at kth instant (x_k) is the error, i.e.

$$e_{k|k} = x_k - \hat{x}_{k|k} \quad (18)$$

The corresponding error at (k-1)th instant can be identified as,

$$e_{k|k-1} = x_k - \hat{x}_{k|k-1} \quad (19)$$

From (11)-(12), the formulations (18)-(19) are as,

$$e_{k|k} = \tilde{F}_{k-1} e_{k-1|k-1} + n_k + l_k \quad (20)$$

$$e_{k|k-1} = F_{k-1} e_{k-1|k-1} + w_{k-1} + r_{k-1} \quad (21)$$

where, r_{k-1} is the remainder term at *(k-1)th* instant ($e_k - F_{k-1}(I_{3\times3} - K_k G_{k-1})e_{k-1}$), and

$$\tilde{F}_{k-1} = \left[I_{3\times3} - K_k G_{k-1}\right] F_{k-1} \quad (22)$$

$$n_k = \left[I_{3\times3} - K_k G_{k-1}\right] w_{k-1} - K_k \varepsilon_k \quad (23)$$

$$l_k = \left[I_{3\times3} - K_k G_{k-1}\right] r_{k-1} \quad (24)$$

$$F_{k-1} = \left.\frac{\partial f}{\partial \hat{x}}\right|_{\hat{x}=\hat{x}_{k|k-1}} ; G_{k-1} = \left.\frac{\partial g}{\partial \hat{x}}\right|_{x_k=\hat{x}_{k|k-1}} \quad (25)$$

With the decent assumptions that the norm $\|F_k\|$ is bounded and $P_{k|k}$ and $P_{k|k-1}$ are bounded with $p_1 I_{3\times3}$, $p_2 I_{3\times3}$ and $q_1 I_{3\times3}$, $q_2 I_{3\times3}$ as respective lower and upper bounds. The following lemmas can be identified to prove the exponential convergence of the algorithm [30].

Lemma-1: With F_k as non-singular $\forall k>0$, and $\|F_k\|$, $P_{k|k}$ and $P_{k|k-1}$ are bounded, then there exist a real number $0 < \lambda < 1$ such that,

$$\tilde{F}_k^T P_{k|k}^{-1} \tilde{F}_k \le (1-\lambda) P_{k|k-1}^{-1} \quad (26)$$

Lemma-2: When the ratio of largest and smallest singular value in 'G_k' matrix has an upper bound 'g', then an upper bound for the norm of the Kalman gain matrix is given as,

$$\|K_k\| \le g(q_2/q_1) \quad (27)$$

Thus, when the error at (k-1)th instant i.e. $\|e_{k-1|k-1}\|$ is bounded, with the bounds (26) and (27), it can be proved that

This article has been accepted for publication in a future issue of this journal, but has not been fully edited. Content may change prior to final publication. Citation information: DOI 10.1109/TIE.2019.2899546, IEEE Transactions on Industrial Electronics

the solution of the error model (20) is exponentially stable with finite bounded limits [30].

B. Assigning Load Current Weights

The active power component of load currents, is then evaluated using a sample and hold (S/H) control logic. The fundamental component estimated from (8)-(17), is passed through S/H logics. Since the fundamental component is in phase with the grid voltages, the triggering pulses for S/H logics are produced using quadrature unit templates, with a zero crossing detector (ZCD). This is described in Fig. 2. For this purpose, the in-phase (x_{pa}, x_{pb}, x_{pc}) and quadrature (x_{qa}, x_{qb}, x_{qc}) unit templates are computed. To achieve satisfactory performance under grid voltage imbalances and harmonic distortions, a new method of extraction of unit templates, is presented here. The mathematical formulation for derivation of enhanced unit templates follows the following sequence.

1) Initially the positive sequence phase voltages are evaluated. The instantaneous positive sequence voltage components in $\alpha\beta$ reference frame are evaluated as,

$$v_{\alpha\beta}^{+}=\left[T_{\alpha\beta}\right]\left[T_{p}\right]\left[T_{\alpha\beta}\right]^{-1}v_{\alpha\beta}=\frac{1}{2}\begin{bmatrix}1 & -e^{-j\pi/2}\\ e^{-j\pi/2} & 1\end{bmatrix}v_{\alpha\beta} \quad (28)$$

$$\left[T_{\alpha\beta}\right]=\sqrt{\frac{2}{3}}\begin{bmatrix}1 & -0.5 & -0.5\\ 0 & 0.866 & -0.866\end{bmatrix} \quad (29)$$

$$\left[T_{p}\right]=\frac{1}{3}\begin{bmatrix}1 & a & a^{2}\\ a^{2} & 1 & a\\ a & a^{2} & 1\end{bmatrix};a=e^{j2\pi/3} \quad (30)$$

Thus, from (28) the positive sequence voltages '$v_{\alpha\beta}^{+}$' and corresponding quantities in *abc*-domain, are evaluated using inverse Clarke's transformation. The implementation of (28) is depicted in Fig. 4. Initially, αβ-components of phase voltages (v_α, v_β) are generated through Clarke's transformation. These are processed through generalized integrators of second order, to obtain corresponding in-phase ($v_{\alpha i}$, $v_{\beta i}$) and quadrature ($v_{\alpha q}$, $v_{\beta q}$) components. The description of second order- second order generalized integrators (SO-SOGI) is reported in [31]. The in-phase and quadrature components are further possessed, as shown in Fig. 4, to evaluate the balanced positive sequence voltage components (v_{sa}^{+}, v_{sb}^{+}, v_{sc}^{+}).

2) The amplitude of terminal voltage is then evaluated as,

$$V_t=\sqrt{(2/3)\left(v_{sa}^{+2}+v_{sb}^{+2}+v_{sc}^{+2}\right)} \quad (31)$$

3) The enhanced in-phase ((x_{pa}^{m}, x_{pb}^{m}, x_{pc}^{m})) and quadrature ((x_{qa}^{m}, x_{qb}^{m}, x_{qc}^{m})) unit templates are then computed as,

$$\mathbf{x_p^m}=\begin{bmatrix}x_{pa}^{m} & x_{pb}^{m} & x_{pc}^{m}\end{bmatrix}^{T}=(1/V_t)\begin{bmatrix}v_{sa}^{+} & v_{sb}^{+} & v_{sc}^{+}\end{bmatrix}^{T} \quad (32)$$

$$\mathbf{x_q^m}=\begin{bmatrix}x_{qa}^{m}\\ x_{qb}^{m}\\ x_{qc}^{m}\end{bmatrix}=\frac{1}{2\sqrt{3}}\begin{bmatrix}0 & -2 & 2\\ 3 & 1 & -1\\ -3 & 1 & -1\end{bmatrix}\begin{bmatrix}x_{pa}^{m}\\ x_{pb}^{m}\\ x_{pc}^{m}\end{bmatrix} \quad (33)$$

Finally, the load current weights (W_{La}, W_{Lb}, W_{Lc}) are obtained from S/H logics output. The average of load current weight, is the equivalent active power component of load current (W_{Leq}).

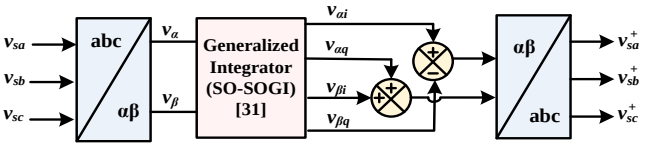

Fig. 4 Evaluation of balanced positive sequence grid voltages

C. DC Link Voltage Regulation and PV Feed-Forward Compensation

The PV inverter necessitates active power to regulate DC link voltage (V_{DC}) to its reference (V_{DC}^{ref}). The VSC consumes some power from common coupling point during variation of the DC link voltage, which is called as loss component of active power (W_{loss}). It is used to regulate DC link voltage according to reference DC link voltage, and isevaluated as,

$$W_{loss}=k_p\left(V_{DC}^{ref}-V_{DC}\right)+k_i\int\left(V_{DC}^{ref}-V_{DC}\right)dt \quad (34)$$

Where, 'k_p' and 'k_i' are the proportional and integral gains of the controller, respectively. The reference voltage for DC link capacitor, is kept 1.2 times the peak of line voltage.

Additionally, PV feed-forward term is incorporated here, to quicken the dynamic response under continuous solar insolation fluctuations that occur in practical PV system.

A practical grid-interfaced PV system is subject to continuous variation of solar isolation. A fast dynamic response is desired under such continuous disturbances to the system. This is facilitated by the feed-forward term (W_{PV}) by minimizing the transients in the grid currents. The PV feed-forward is an additional term accommodated in the control strategy, which adjusts the reference grid currents without any feedback from the controller, to improve the dynamic performance of grid currents during the changes in solar insolation. Since the dynamics are directly associated with the change in PV array power (P_{PV}), 'W_{PV}' can be identified as,

$$W_{pv}={(2P_{PV})}/{(3V_t)} \quad (35)$$

D. Fault Ride-Through Control

The proposed fault ride-through control of PV inverter is demonstrated in this section. The three phase voltages are expressed in $\alpha\beta$ reference frame using Clarke's transformation matrix depicted in (36) (where $\mathbf{u}_{\alpha\beta}$ is vector in $\alpha\beta$ reference frame and $\mathbf{u}_{abc}$ is vector in *abc* reference frame),

$$\mathbf{u}_{\alpha\beta}=\mathbf{T}_{abc}^{\alpha\beta}\mathbf{u}_{abc};\quad \mathbf{T}_{abc}^{\alpha\beta}=\sqrt{\frac{2}{3}}\begin{bmatrix}1 & -1/2 & -1/2\\ 0 & \sqrt{3}/2 & -\sqrt{3}/2\end{bmatrix} \quad (36)$$

The αβ-voltage components, 'v_α' and 'v_β' are used to compute their respective positive and negative sequence voltages as follows,

$$\begin{bmatrix}v_\alpha^{+}\\ v_\beta^{+}\\ v_\alpha^{-}\\ v_\beta^{-}\end{bmatrix}=\frac{1}{2}\begin{bmatrix}1 & -e^{-j\pi/2}\\ e^{-j\pi/2} & 1\\ 1 & e^{-j\pi/2}\\ -e^{-j\pi/2} & 1\end{bmatrix}\begin{bmatrix}1 & -1/2 & -1/2\\ 0 & \sqrt{3}/2 & -\sqrt{3}/2\end{bmatrix}\begin{bmatrix}v_{sa}\\ v_{sb}\\ v_{sc}\end{bmatrix} \quad (37)$$

The positive sequence voltage (V^{+}), negative sequence voltage (V^{-}) and the per-unit voltage (V_{pu}) are then computed as follows,

This article has been accepted for publication in a future issue of this journal, but has not been fully edited. Content may change prior to final publication. Citation information: DOI 10.1109/TIE.2019.2899546, IEEE Transactions on Industrial Electronics

$$V^{+}=\sqrt{v_{\alpha}^{+2}+v_{\beta}^{+2}};V^{-}=\sqrt{v_{\alpha}^{-2}+v_{\beta}^{-2}}$$
$$V_{pu}=\left(\sqrt{3}/\sqrt{2}V_{n}\right)\sqrt{v_{\alpha}^{2}+v_{\beta}^{2}};\ \bar{V}_{pu}=Mean\left(V_{pu}\right) \quad (38)$$

where 'V_n' is the nominal converter voltage. The over currents caused due to the near PCC faults, trip the interfacing power converter thereby leading to the loss in entire solar PV generation. To avoid such failures, inverter nominal power must be updated under low voltages. Therefore, a modified nominal power (*MNP*) [23], is adopted here, which is a function of voltage sag depth and nominal converter power (S_n) as,

$$MNP=\left(1/V_{n}\right)\left(V^{+}-V^{-}\right)S_{n} \quad (39)$$

Under low voltage faults in the system, the modified power is updated to take a value lower than the nominal power of the converter. The decrease in voltage magnitudes of either single phase, double phase or three phase voltages, results in a decrease in the value of *MNP*. This is demonstrated in more detailed in the simulation results. As per the depth of voltage drop, the estimated reactive power entering the grid (Q_{gE}) to be supplied by the converter is decided as follows [32],

$$Q_{gE}=\begin{cases}0 & \text{if } \bar{V}_{pu}>0.9\\ \left(1.35-1.5V_{pu}\right)S_{n} & \text{if } 0.2<\bar{V}_{pu}<0.9\\ 1.05S_{n} & \text{if } \bar{V}_{pu}<0.2\end{cases} \quad (40)$$

Thus the maximum active power injection, for a given value of MNP and reactive power can be identified as,

$$P_{\max}=\begin{cases}\sqrt{MNP^{2}-Q_{gE}^{2}} & \text{if } MNP>Q_{gE}\\ 0 & \text{if } MNP<Q_{gE}\end{cases} \quad (41)$$

Under normal conditions, the reference grid reactive power (Q_{gref}) is 'Q_{gE}', governed by (40), However, under very deep voltage sags, the VSI is incapable of injecting the reactive power higher than the MNP, and therefore, the converter is made to supply reactive power equal to MNP. Thus,

$$Q_{\text{gref}}=\begin{cases}Q_{gE} & \text{if } Q_{gE}\le MNP\\ MNP & \text{if } Q_{gE}>MNP\end{cases} \quad (42)$$

Therefore, as long as, the P_{max} *i.e.* (41) is higher than the maximum power point reference (P_{ref}) provided by the MPPT controller, the maximum power can be injected from the PV array to the grid. As mentioned earlier, an InC algorithm [28] is used for maximum power point tracking purpose, where the direction of perturbation to reach maximum power point is decided by the difference between the incremental conductance (dI_{PV}/dV_{PV}) and the conductance (I_{PV}/V_{PV}) offered by the PV array. When the difference is positive, it identifies the operating point as left of the PV curve and tries shift the operating point to the right. The visa-versa is true in the case when the difference is negative. Thus, the reference PV array voltage is estimated based on the InC principle the corresponding duty ratio of the boost converter is evaluated. However, if P_{max} is lower than the P_{ref}, then the PV array is made to operate in de-rated mode, at a new operating point corresponding to a new value of active power i.e. P_{max}. The de-rated operation of PV array is depicted in Fig. 5, where the boost converter is controlled to operate in non-MPPT mode. As

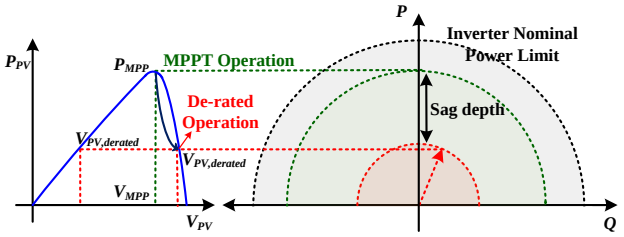

Fig. 5 De-rated operation of PV inverter during fault ride-through operation

shown in Fig. 5, the right hand side operating point is considered here, as the operating point can move faster on the high ramp side of the P-V curve. The reference duty ratio of the boost converter is thus obtained under normal and de-rated conditions as follows,

$$D_{normal}=1-\left(V_{PV}^{ref}/V_{DC}\right) \quad (43)$$
$$D_{derated}=\left(P_{\max}/P_{ref}\right)\left(1-\left(V_{PV}^{ref}/V_{DC}\right)\right) \quad (44)$$

where 'V_{PV}^{ref}' is the reference PV-array voltage provided by the MPPT controller. The control of the boost converter is demonstrated in Fig. 6. Under normal conditions, the boost converter is made to operate in MPPT mode. However, the de-rated operational mode is activated as soon as low voltage is detected (below 0.9pu) and P_{max}<P_{ref}. The duty ratio thus obtained, is compared with the high frequency carrier signal for the generation of switching pulses to the boost converter. The proportional-integral controller in de-rated operation, tunes new duty cycle to precisely follow 'P_{max}'.

E. Generation of Inverter Gating Pulses

The gating pulses for PV inverter, are generated using active and reactive reference grid currents. For this purpose, the net active power component (W_{net}) is evaluated. The net active power component of current component, is amplitude of reference grid currents. This is estimated by summation of equivalent load active power component weight with the amplitude of reference inverter currents (45), in accordance with the Kirchhoff current law at PCC. Thus 'W_{net}' can be identified as,

$$W_{net}=W_{eq}+W_{loss}-W_{pv} \quad (45)$$

Since 'W_{net}' is the net active current weight, the reference active power delivered by the grid (P_{gref}) is obtained by multiplying 'W_{net}' with $\sqrt{3}V_{pu}V_{n}/\sqrt{2}$. Where, '$V_n$' is the nominal grid voltage. This is because the active current weight (W_{net}) is the peak amplitude of the active current, i.e. $P_{g}=\sqrt{3}V_{rms}I_{active,rms}=\left(\sqrt{3}V_{pu}V_{n}/\sqrt{2}\right).W_{net}$.

The active reference currents are then evaluated as,

$$\mathbf{i_p^{ref}}=\begin{bmatrix}i_{pa}^{ref} & i_{pb}^{ref} & i_{pc}^{ref}\end{bmatrix}^{T}=W_{net}.\mathbf{x_p^{m}} \quad (46)$$

To evaluate the reactive reference currents, the reactive current weight (W_q) is obtained by scaling the reference reactive power determined from (42) with the magnitude of terminal voltage. The reactive reference currents are then obtained as,

This article has been accepted for publication in a future issue of this journal, but has not been fully edited. Content may change prior to final publication. Citation information: DOI 10.1109/TIE.2019.2899546, IEEE Transactions on Industrial Electronics

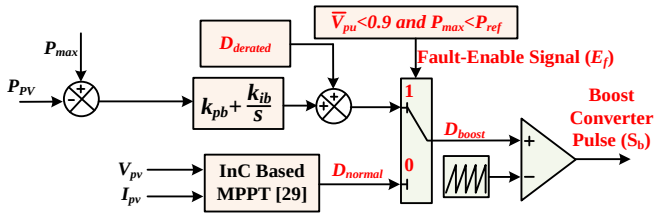

Fig. 6 Control schematic for generation of boost converter gating pulses

$$\mathbf{i}_{\mathbf{q}}^{\mathbf{ref}} = \begin{bmatrix} i_{qa}^{ref} & i_{qb}^{ref} & i_{qc}^{ref} \end{bmatrix}^T = W_q.\mathbf{x}_{\mathbf{q}}^{\mathbf{m}} \quad (47)$$

Finally, the reference grid currents are generated as,

$$\mathbf{i}_{\mathbf{s}}^{\mathbf{ref}} = \begin{bmatrix} i_{sa}^{ref} & i_{sb}^{ref} & i_{sc}^{ref} \end{bmatrix}^T = \mathbf{i}_{\mathbf{p}}^{\mathbf{ref}} + \mathbf{i}_{\mathbf{q}}^{\mathbf{ref}} \quad (48)$$

The error between reference grid currents (48) and the sensed grid currents, is infiltrated through the hysteresis current controller (HCC) to produce the inverter gating pulses. The hysteresis band-width (δ) is reported in Appendix.

IV. Comparative Study With Existing Algorithms

Different control approaches for both grid-interfaced distributed generation systems and specifically solar-PV systems with their advantages/ disadvantages, are analyzed in introduction section. With fault ride through capability, the control strategies [21]-[22] for PV system involve multifunctional feature. On the other hand, the controller actions of proposed controller are discussed in section-III. A comparison is made herein with the multifunctional strategies [21]-[22], from the functionalities point of view. The topology proposed by [21] is for neutral-point clamped inverter. The proposed control strategy is proposed for distribution level system. From functionalities point of view, both approaches [21]-[22] have achieved inverter reference current control with reactive power injection during both balanced/unbalanced voltage sages, while ensuring the inverter peak current limit capability. However, the proposed strategy is advantageous over these controllers as it offers significant additional functionalities, which include harmonic currents mitigation, power factor correction and balancing of grid currents. Moreover, unlike the conventional algorithms, the system operation with the proposed strategy, is not affected by abnormal/harmonic grid voltages caused at far radial ends in the distribution system. The comparative study highlighting different functionalities of the proposed control strategy is reported in Table-I.

V. System Response Under Grid-Side Faults

To verify the proposed control scheme, a simulation test-bed is built in MATLAB®-Simulink based environment with Simscape toolbox. A 415V, 50Hz system is considered here, with DC link voltage of 1.2 times the peak of line voltage. The PV module parameters considered for simulation purpose, are reported in Table-II. The detailed system and control parameters considered for simulation purpose, are reported in Appendix. This section describes the system performance under grid-side faults, highlighting the salient signals.

The performance of grid interfaced PV system under low voltage faults, is depicted in Fig. 7. The simulation parameters are reported in Appendix. Single line to ground (L-G) and

TABLE I

Comparative Study with Fault Ride Through Algorithms

Parameter	Proposed EKF Based Control Strategy	Control Strategy-[21]	Control Strategy-[22]
System Topology	3-leg VSI	3-level NPC Inverter	3-leg VSI
Application	Distribution Grids	MV Grids	MV Grids
Reactive Power Injection during Voltage Sags	Supported	Supported	Supported
Inverter Peak Current Limit Capability	Supported	Supported	Supported
Grid Harmonic Current Elimination	Supported	Not Supported	Not Supported
Performance under Harmonic/Distorted Grid Voltages	Not Affected	Affected	Affected
Balancing of Grid Currents	Supported	Not Supported	Not Supported
PLL Requirement in Control Strategy	Not Required	Required	Not Required

TABLE II

Parameters of PV Module

Parameter	Value	Parameter	Value
Open Circuit Voltage (V_{oc})	32.9 V	Maximum Power (P_{pvmax})	200.1 W
Short-Circuit Current (I_{sc})	8.21 A	Series Resistance (R_s)	0.215 Ω
MPP Voltage (V_{mpp})	26.3 V	Parallel Resistance (R_p)	415.415 Ω
MPP Current (I_{mpp})	7.61 A	Cells per Module (N_{cell})	54
No. of Series Modules (N_s)	17	No. of Parallel Modules (N_p)	9

double-line to ground (L-L-G) faults, are simulated at 1s and 1.1s, respectively. Upon the occurrence of the fault, the per-unit voltage falls to 0.6pu. A severe L-L-G fault is then simulated at 1.2s where the grid voltages fall as low as 0.1pu. The salient signals of grid voltages (v_g), $V^+ - V^-$,V_{pu}, MNP, P_{max}, Q_g, D_{normal}, D_{boost}, P_{PV}, V_{PV}, grid currents (i_g) and VSC currents (i_{VSC}) are depicted in Fig. 7. As soon as fault signal is detected by the algorithm, $V^+ - V^-$, MNP and P_{max} are updated as per (38),(39) and (41), respectively. These are shown in Fig. 7(a). The reactive power injected to the grid, follows the reference reactive power (42), and thereby provides the reactive power support under low voltage faults. As soon as the MNP falls below the rated power of power converter (35 kVA), the de-rated PV array operation mode is enabled. Consequently, the duty ratio is updated as per (43)-(44) (Fig. 6). The PI control parameters (k_{pb} and k_{ib}) are reported in Appendix. Accordingly, the dynamics in duty ratio of the boost

This article has been accepted for publication in a future issue of this journal, but has not been fully edited. Content may change prior to final publication. Citation information: DOI 10.1109/TIE.2019.2899546, IEEE Transactions on Industrial Electronics

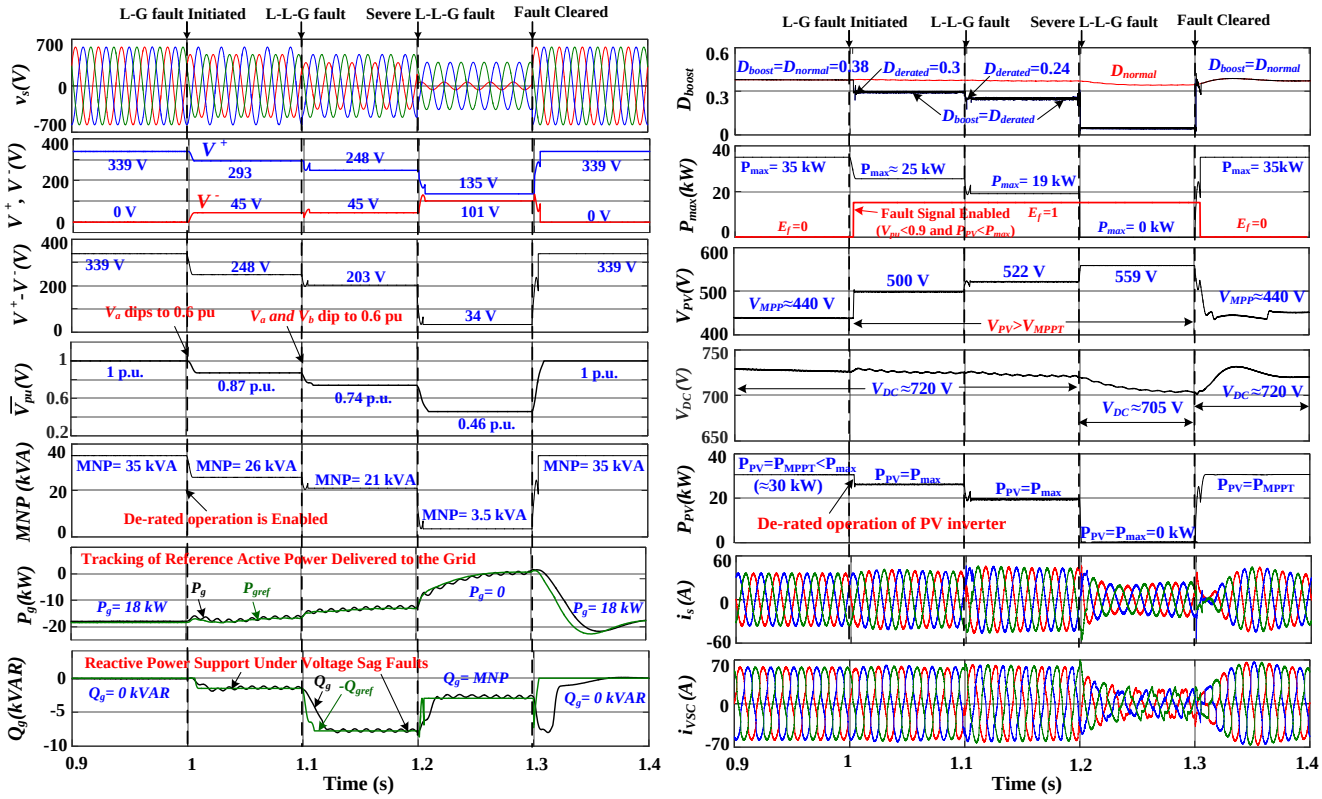

(a) (b)

Fig. 7 System response under L-G and L-L-G faults depicting fault ride-through operation of PV inverter

converter (D_{boost}), PV voltage (V_{PV}) and PV array power (P_{PV}) are observed as shown in Fig. 7(b). Before the occurrence of the fault, the PV array operates at its MPP of 440V and 30kW, however, the PV power is limited to P_{max}(25kW and 19kW), after the occurrence of faults at 1s and 1.1s, and V_{PV} is shifted to a new operating points at 500V and 522V, respectively. It may be noted from Figs. 7(a)-(b) that, under severe grid faults (at 1.2s), the reactive power entering the grid (Q_g) is limited to MNP (3.5 kVA). In this case, no active power supplied by the PV inverter, with zero duty-ratio of the boost converter; thus, the PV inverter simply acts as a static compensator. Despite the unbalanced voltage faults, the grid currents always remained balanced and sinusoidal with THD less than 5%, as the compensating currents are provided by the PV inverter under all conditions.

VI. Experimental Results

A prototype of grid interfaced PV system is developed in the laboratory to validate the control scheme. The solar power generation is emulated using solar PV emulator (Ametek make). The Hall Effect current sensors (LA55-P) and Hall Effect voltage sensors (LA25-P) are utilized for current and voltage sensing, respectively. The optocouplers are used for isolation purpose between DSP signal and VSC. The proposed control strategy is realized with digital-signal-processor (DSP) dSPACE-1202 microlab-box controller. The behavior of PV system is recorded and analyzed through a power analyzer (Fluke: model 43-B) and four channel oscilloscope (Aglient make). The steady state and dynamic performances of the proposed system, are demonstrated with respect to the dynamic changes in grid and load side network. The behavior of the system is analyzed using in terms of DC link voltage (V_{DC}), PV-array voltage (V_{PV}), grid line voltages (v_{sab}, v_{sbc}, v_{sca}) reference currents (i_{sa}^*, i_{sb}^*, i_{sc}^*) extraction, PV array power (P_{PV}), VSC currents (i_{VSC}), grid currents (i_s), PV feed forward component (W_{pvff}) and load currents (i_L).

A. Steady-state Response of the System

Fig. 8 shows the performance of the system under balanced nonlinear load connected at PCC. Figs. 8(a)-(c) depict the voltage and current waveforms of grid, inverter and load. Fig 8(d) depicts the harmonic spectrum of load current. Figs. 8(e)-(g) show the power flow through grid, power supplied by the

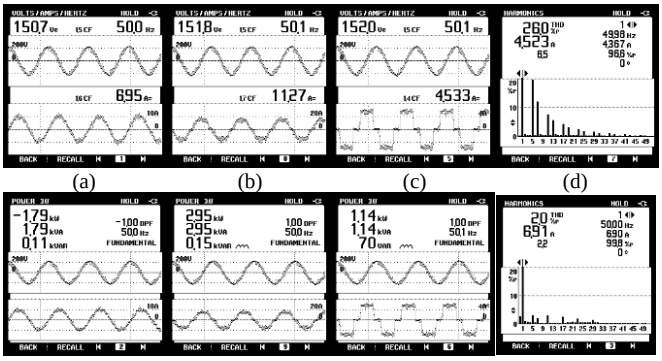

(a) (b) (c) (d)

(e) (f) (g) (h)

Fig. 8 Test results under nonlinear loads (a) v_{sab}-i_{sa} (b) v_{sab}-i_{vsca} (c) v_{sab}-i_{La} (d) THD of i_{La} (e) Grid Power (f) Inverter Power (g) Load Power (h) THD of i_{sa}

This article has been accepted for publication in a future issue of this journal, but has not been fully edited. Content may change prior to final publication. Citation information: DOI 10.1109/TIE.2019.2899546, IEEE Transactions on Industrial Electronics

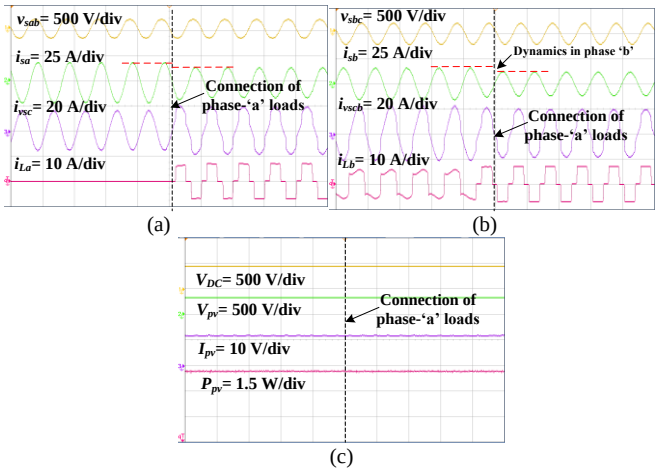

Fig. 9 System behaviour under load balancing (a)v_{sab}, i_{sa}, i_{vsca}, i_{La} (b) v_{sbc}, i_{sb}, i_{vscb}, i_{Lb} (c) V_{DC}, V_{pv}, I_{pv}, P_{pv}

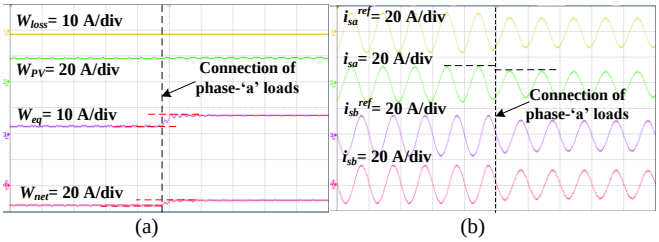

Fig. 10 Salient internal signals of the controller-(a) W_{loss}, W_{PV}, W_{eq}, W_{net} and (b) reference currents - i_{sa}^{*}, $i_{sa,}$ i_{sb}^{*}, i_{sb}

PV inverter and power consumption of the load. The arithmetic sum of load power and grid power is equal to PV inverter system, which illustrates that PV array coupled VSC supplies power to load as well as to the distribution network. The THD of grid current is achieved 2% despite the load current THD of 26%, which as shown in Figs. 8(d) and 8(h).

B. System Performance under Dynamic Loads

The system behavior under unbalanced nonlinear loads, balanced nonlinear loads and the transition between both is shown in Figs. 9(a)-(c). The dynamic operation is realized by phase-'a' load reconnection. Fig. 9 (a) shows the dynamics in v_{sab}, i_{sa}, i_{vsca}, i_{La}. and Fig. 9(b) depicts v_{sbc}, i_{sb}, i_{vscb}, i_{Lb}. The PV array parameters are depicted in Fig. 9(c), along with DC-link voltage. The grid currents remain sinusoidal and balanced at both balanced and unbalanced nonlinear loads. The DC link voltage is maintained regulated, tracking the reference DC link voltage. The power extraction from PV array is least affected by load-side network changes.

To validate the behavior of the proposed controller, salient internal signals are recorded. Fig. 10(a) shows effectiveness of EKF algorithm in fundamental extraction, in terms of the variation in weight components- W_{eq}, W_{loss}, W_{PV} and W_{net}. The load current component is increased, accounting for phase-'a' load current and consequently, the net amplitude of reference currents, is increased. Fig. 10(b) depicts the reference current generation of the controller. The reference currents decrease under load connection as extra load power causing from the load connection, is supplied by PV-inverter, and consequently reduced power is fed to the grid. The grid reference currents tracking capability is also depicted in Fig. 10(b).

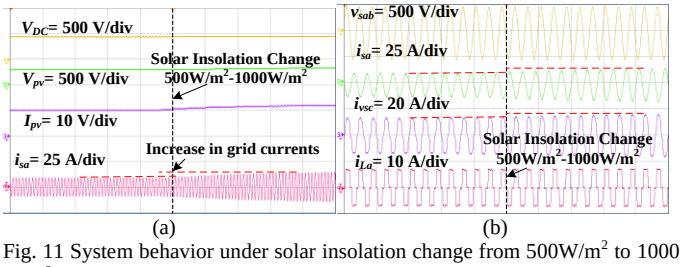

Fig. 11 System behavior under solar insolation change from 500W/m^2 to 1000 W/m^2 (a) v_{sab}, i_{sa}, i_{vsca}, i_{La} (b) V_{DC}, V_{pv}, I_{pv}, P_{pv}

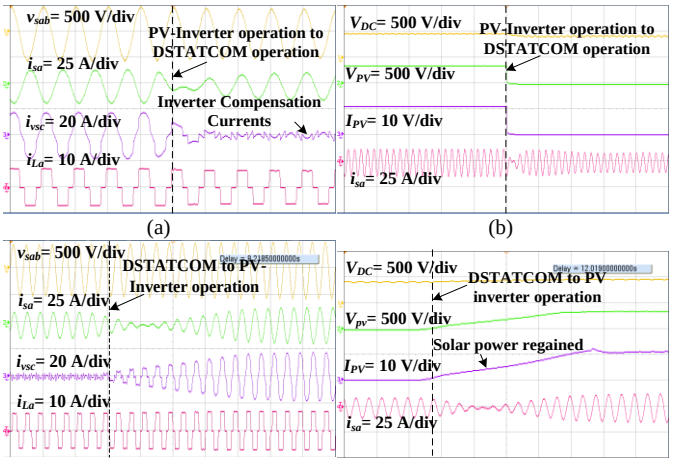

Fig. 12 Behavior under transitions between grid-interfaced PV operation and DSTATCOM operation (a) v_{sab}, i_{sa}, i_{vsca}, i_{La} (b) V_{DC}, V_{pv}, I_{pv}, P_{pv}; and vice-versa (c) v_{sab}, i_{sa}, i_{vsca}, i_{La} (d) V_{DC}, V_{pv}, I_{pv}, P_{pv}

C. System Performance under Changes in Solar Insolation

The performance of the system, is analyzed as solar insolation variation from 500W/m^2 to 1000W/m^2 and vice versa. The response is recorded in terms of PV-array voltage (V_{PV}), PV-array current (I_{PV}), inverter current (i_{VSCa}) and source current (i_{sa}), as shown in Figs. 11(a) and 11(b). The increased PV array power resulting from insolation change is fed back to the grid, thereby resulting in increased grid currents. The DC bus voltage is least affected.

D. Transitions between Grid-Interfaced PV Operation and DSTATCOM Operation

During night times, when the solar PV array is incapable of generating power, the control strategy automatically adapts to the change in system configuration from grid-interfaced PV system to DSTATCOM. The system performance depicting this operation, is shown in Figs. 12(a)-(b), in terms of v_{sab}, i_{sa}, i_{vsca}, $i_{La,}$ V_{DC}, V_{pv}, I_{pv}. During the transition, the phase inversion of grid currents, is observed (power flow direction is reversed), as a result of compensating currents supplied by the inverter under the presence of nonlinear loads at PCC, as depicted in Fig. 12(a). The DC link voltage is regulated at its reference value as shown in Fig. 12(b). Figs. 12(c)-(d) demonstrate the system behavior under vice-versa operation i.e. from DSTATCOM to grid-interfaced solar PV operation.

E. System Performance under Distorted Grid Voltages

The system performance under distorted grid voltage conditions, is shown in Figs. 13(a)-(d). In practical scenarios, the distortion in grid voltages, is observed at far radial ends where the grid voltages suffer huge diversions. Fig. 13(a)

This article has been accepted for publication in a future issue of this journal, but has not been fully edited. Content may change prior to final publication. Citation information: DOI 10.1109/TIE.2019.2899546, IEEE Transactions on Industrial Electronics

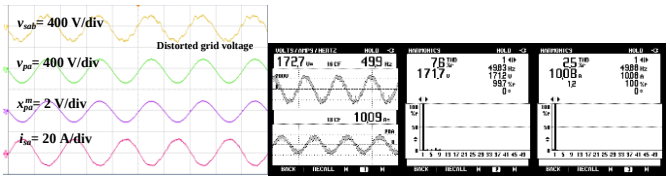

(a) (b) (c) (d)

Fig. 13 Behavior under distorted grid voltages (a) v_{sab}, v_{pa}, u_{pa}, i_{sa} (b) v_{sab}-i_{sa} (c)-(d) THDs of v_{sab} and i_{sa}

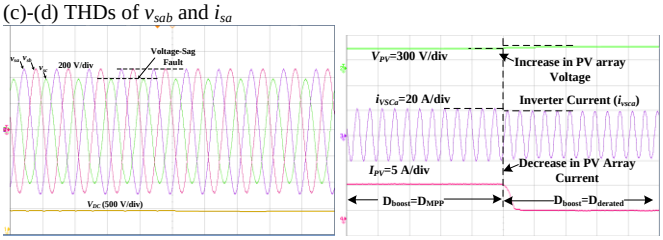

(a) (b)

Fig. 14 Behavior under voltage-sag fault (a) v_{sa},$v_{sb}$and v_{sc}(b) V_{PV}, I_{PV} and I_{VSCa}

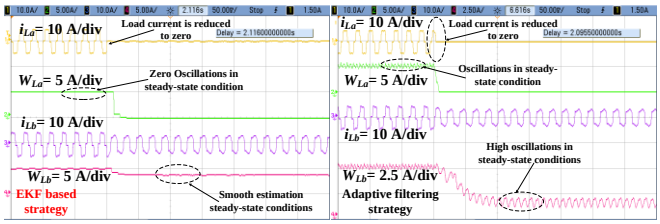

(a) (b)

Fig. 15 Comparative performance of fundamental component magnitude estimation using (a) proposed EKF strategy (b) adaptive filtering strategy [27]

depicts the salient signals of v_{sab}, v_{pa}, x_{pa} and i_{sa}. The grid voltage (v_{sab}) and grid current (i_{sa}) during the voltage distortions, are shown in Fig. 13(b) and the harmonic spectrum of grid voltage is shown in Fig. 13(c). As illustrated in Fig. 4, only the balanced positive sequence of the phase voltages extracted using the second order generalized integrators, are considered for derivation of unit templates. For this reason, the unit templates thus derived have no distortions despite distorted grid voltages and consequently, the reference gridcurrents are least affected by the distortion in grid voltages. Thus, as depicted in Fig. 13(d), the grid currents THD is thus observed 2.5%, within the limits recommended by the IEEE-519 standard for harmonic current control in area EPS (Electric Power System).

E. System Performance under Voltage Sag Fault

To verify the system performance under fault condition, an unbalanced voltage-sag is created, where the phase-'c' voltage is dropped to 0.8 p.u, as shown in Fig. 14(a). The dynamics in PV array current, voltage and inverter current during sudden dip in grid voltages, is shown in Fig. 14(b). An increase in PV array voltage and decrease in PV array power, are observed, due to the shift in the operating point to the right of P-V characteristic curve. Consequently, PV inverter is operated in de-rated mode and the boost converter is operated with duty ratio '$D_{derated}$', as depicted in Fig. 5 and Fig. 6. A decrease in inverter currents is observed, accounting to decrease in PV array power output at de-rated operating point.

F. Effectiveness of EKF algorithm

Figs. 15(a)-(b) depict the comparative performance between proposed EKF based algorithm and conventional adaptive filtering technique, during steady-state conditions and during load perturbation. The effectiveness of proposed algorithm in estimation of the fundamental load current magnitude is shown, in comparison with least mean square/fourth (LMS/F) based adaptive filtering strategy [26]. As depicted in Fig. 15(b), the fundamental load current magnitude estimation using adaptive filtering technique is oscillatory, because the error in the algorithm has been cubed. As the algorithm is approaches the desired steady-state value, it becomes insensitive to the error. Since the step size is fixed, the weights in the adaptive filtering algorithm practically, stop updating after reaching within certain error limits, and therefore the steady-state response of the algorithm is always oscillatory. On the other hand, upon choosing higher value of step size in adaptive filtering technique, the dynamic response is affected. Thus the estimation of the fundamental magnitude of load currents, is affected, and consequently the estimated amplitude of the load current fundamental (W_{La}, $W_{Lb,}$ W_{Lc}) is affected, as depicted in Fig. 15(b) for phase-'a' and phase-'b'. Thereby, it affects the system performance by increasing the harmonic content in the reference grid currents. However, the proposed EKF based strategy precisely estimates the load fundamental magnitude, thereby, resulting in smooth steady-state and dynamic responses.

VII. CONCLUSION

The EKF state-estimator based control strategy is proposed for fault ride through operation in two-stage grid interfaced PV system, which enables the load compensation features in three phase distribution system. The converter over-currents caused due to low voltage sags in the GPV system, are avoided, by providing an auxiliary reactive power support as recommended by IEEE Standard-1547.4. Here, the ride-through operation is achieved without compromising the load compensation features such as grid harmonic currents elimination, grid currents balancing and power factor correction. For ride-through purpose, a maximum safe limit of PV power injection is derived as a function of grid-voltage sag and the PV inverter rating. The de-rated operation of PV array is enabled, in cases when the maximum PV power becomes higher than the maximum safe limit of active power injection. To achieve this, the mechanism for a boost converter duty-ratio control, is presented. The reactive power is then injected to the grid under voltage sag faults, as per the depth in voltage-sag. The simulation results under LG and LLG faults, demonstrate the effectiveness of proposed control scheme. Despite the unbalanced faults, the grid currents remain balanced and sinusoidal, thereby, the negative sequence and zero sequence power injection to the grid are avoided. Test results validate proposed control strategy. The features of harmonic currents mitigation, reactive power compensation, grid currents balancing and power factor correction, are illustrated under various test conditions. The results under distorted grid voltages and L-G unbalanced fault, are also presented. Under both normal and abnormal grid conditions, the grid currents with proposed control strategy, are balanced and are maintained within the THD limit recommended by the IEEE standard-519. The practical grid interfaced PV systems, are

subject to continuous grid side perturbations and proposed control strategy serves as a possible solution, owing to its multi-functional features and self-adaptation capability to the variations in grid-side parameters.

APPENDIX

A. Simulation System Parameters:

Grid voltage=415 V; L_s= 0.2*m*H/phase and R_s = 0.04 Ω/phase; *f*= 50 Hz; R_L = 25Ω, L_L = 100 *m*H; Boost Inductor = 5 *m*H; DC capacitor C_{DC} = 4700 μF; Interfacing inductor L_f = 4*m*H; Ripple filter: *R*=10Ω, *C* = 80μF; δ=0.1; Parameters of PV module: *As reported in Table-II*; DC voltage Controller: k_p=0.2 and k_i=0.01.

B. Experimental System Parameters:

Grid voltage= 150V; ω=314 rad/s; Nonlinear loads: diode bridge rectifier with 60 Ω and 200 *m*H;V_{oc}=330 V, I_{sc}=15.3 A,I_{mpp}=12.8 A,V_{mpp}=280V, Interfacing inductor (L_f) = 3.5*m*H, DC bus capacitor (C_{dc}) =2200 μF, Ripple Filter= 5.5 Ω , 10μF.

REFERENCES

[1] E.Hache, A. Palle, "Renewable energy source integration into power networks, research trends and policy implications: A bibliometric and research actors survey analysis", Energy Policy, vol. 124, pp. 23-35, 2019.

[2] B. Singh, A. Chandra, and K. Al-Haddad, Power Quality: Problems and Mitigation Techniques. Hoboken, NJ, USA: Wiley, Jan. 2015.

[3] V. L. Srinivas, S. Kumar, S. Bhim and S. Mishra, "A Multifunctional GPV System Using Adaptive Observer Based Harmonic Cancellation Technique," *IEEE Trans.Ind. Electron.*, vol. 65, no. 2, pp. 1347-1357, 2018..

[4] S. Bhim and J. Solanki, "A comparison of control algorithms for DSTATCOM," *IEEE Trans. Ind. Electr.*, vol. 56, no. 7, pp. 2738-2745, July 2009.

[5] Q. Chen, X. Luo, L. Zhang and S. Quan, "Model predictive control for three-phase four-leg grid-tied inverters," *IEEE Access*, vol. 5, pp. 2834-2841, 2017.

[6] K. K. Shyu, M. J. Yang, Y. M. Chen and Y. F. Lin, "Model Reference Adaptive Control Design for a Shunt Active Power Filter System," in *Proc. IECON 2006 - 32nd Annual Conference on IEEE Industrial Electronics*, Paris, 2006, pp. 73-78.

[7] W. Fei, J. L. Duarte, and M. A. M. Hendrix, "Pliant active and reactive power control for grid-interactive converters under unbalanced voltage dips," *IEEE Trans. Pow. Electr.*, vol. 26, no. 5, pp. 1511–1521, 2011.

[8] H. S. Song and K. Nam, "Dual current control scheme for PWM converter under unbalanced input voltage conditions," *IEEE Trans. Ind. Electron.*, vol. 46, no. 5, pp. 953–959, Oct. 1999.

[9] M. Reyes, P. Rodriguez, S. Vazquez, A. Luna, R. Teodorescu, and J. M. Carrasco, "Enhanced decoupled double synchronous reference frame current controller for unbalanced grid-voltage conditions," *IEEE Trans. Power Electron.*, vol. 27, no. 9, pp. 3934–3943, Sep. 2012.

[10] A. Camacho, M. Castilla, J. Miret, A. Borrell, and L. de Vicuna, "Active and reactive power strategies with peak current limitation for distributed generation inverters during unbalanced grid faults," *IEEE Trans. Ind. Electron.*, vol. 62, no. 3, pp. 1515-1525, Mar. 2015.

[11] A. Camacho, M. Castilla, J. Miret, J. Vasquez, and E. Alarcon-Gallo, "Flexible voltage support control for three phase distributed generation inverters under grid fault," *IEEE Trans. Ind. Electron.*, vol. 60, no. 4, pp. 1429–1441, 2013.

[12] J. Miret, A. Camacho, M. Castilla, L. G. de Vicuna, and J. Matas, "Control scheme with voltage support capability for distributed generation inverters under voltage sags," *IEEE Trans. Power Electron.*, vol. 28, no. 11, pp. 5252–5263, Nov. 2013.

[13] C. T. Lee, C. W. Hsu, and P. T. Cheng, "A low-voltage ride-through technique for grid-connected converters of distributed energy resources," *IEEE Trans. Ind. Appl.*, vol. 47, no. 4, pp. 1821–1832, 2011.

[14] M. Castilla, J. Miret, A. Camacho, J. Matas, and L. Garcia de Vicuna, "Voltage support control strategies for static synchronous compensators under unbalanced voltage sags," *IEEE Trans. Ind. Electron.*, vol. 61, no. 2, pp. 808–820, Feb. 2014.

[15] Y. Suh and T. A. Lipo, "Control scheme in hybrid synchronous stationary frame for PWM AC/DC converter under generalized unbalanced operating conditions," *IEEE Trans. Ind. Appl.*, vol. 42, no. 3, pp. 825–835, May/ Jun. 2006.

[16] Z. Li, Y. Li, P. Wang, H. Zhu, C. Liu, and W. Xu, "Control of three-phase boost-type PWM rectifier in stationary frame under unbalanced input voltage," *IEEE Trans. Power Electron.*, vol. 25, no. 10, pp. 2521–2530, Oct. 2010.

[17] P. Rodriguez, A. V. Timbus, R. Teodorescu, M. Liserre, and F. Blaabjerg, "Flexible active power control of distributed power generation systems during grid faults," *IEEE Trans. Ind. Electron.*, vol. 54, no. 5, pp. 2583–2592, Oct. 2007.

[18] F. Wang, J. L. Duarte, and M. A. M. Hendrix, "Pliant active and reactive power control for grid-interactive converters under unbalanced voltage dips," *IEEE Trans. Pow. Electr.*, vol. 26, no. 5, pp. 1511–1521, 2011.

[19] M. Mirhosseini, J. Pou, V. G. Agelidis, 'Individual phase current control with the capability to avoid overvoltage in grid-connected photovoltaic power plants under unbalanced voltage sags', *IEEE Trans. Power Electron.*, vol. 30, no. 10, pp 5346–5351, 2015.

[20] Y. Yang, H. Wang, F. Blaabjerg and T. Kerekes, "A Hybrid Power Control Concept for PV Inverters With Reduced Thermal Loading," *IEEE Trans. Pow. Electron.*, vol. 29, no. 12, pp. 6271-6275, Dec. 2014.

[21] H. D. Tafti, A. Maswood, G. Konstantinou, J. Pou, K. Kandasamy, Z. Lim, and G. H. P. Ooi, "Study on the low-voltage ride-thorough capability of photovoltaic grid-connected neutral-point-clamped inverters with active/reactive power injection," *IET Renew. Pow. Gen.*, vol. 11, pp. 1182–1190, July 2017.

[22] D. Hossein, A. Iftekhar, K. Georgios, P. Josep and P. Acuna, "Active/reactive power control of photovoltaic grid-tied inverters with peak current limitation and zero active power oscillation during unbalanced voltage sags," *IET Power Electron.*, vol. 11, no. 6, 2018.

[23] E. Afshari, Gholam R. Moradi, R. Rahimi, B. Farhangi, Y. Yang ; F. Blaabjerg and S.Farhangi, "Control Strategy for Three-Phase Grid-Connected PV Inverters Enabling Current Limitation Under Unbalanced Faults," *IEEE Trans. Ind. Electr.*, vol. 64, no. 11, pp. 8908-8918, 2017.

[24] N. Zhang, H. Tang, and C. Yao, " A systematic method for designing a PR controller and active damping of the LCL filter for single-phase grid-connected PV inverters", *Energies*, vol.7, no. 6, pp.3934-3954, 2014.

[25] F. Wu, D. Sun, L. Zhang and J. Duan, "Influence of plugging DC offset estimation integrator in single-phase EPLL and alternative scheme to eliminate effect of input DC offset and harmonics," *IEEE Trans. Ind. Electron.*, vol. 62, no. 8, pp. 4823-4831, Aug. 2015.

[26] U. Subudhi, H. K. Sahoo and S. K. Mishra, "Harmonics and Decaying DC Estimation Using Volterra LMS/F Algorithm," in *IEEE Trans. Ind. Appl.*, vol. 54, no. 2, pp. 1108-1118, March-April 2018..

[27] N. Kishor, S. R. Mohanty, M. G. Villalva and E. Ruppert, "Simulation of PV array output power for modified PV cell model," in *Proc. IEEE Int. Conf. on Power and Energy*, Kuala Lumpur, pp. 533-538, 2010.

[28] M. A. G. de Brito, L. Galotto, L. P. Sampaio, G. d. A. e Melo and C. A. Canesin, "Evaluation of the Main MPPT Techniques for Photovoltaic Applications," in *IEEE Transactions on Industrial Electronics*, vol. 60, no. 3, pp. 1156-1167, March 2013.

[29] G. Anagnostou and B. C. Pal, "Derivative-Free Kalman Filtering Based Approaches to Dynamic State Estimation for Power Systems With Unknown Inputs," *IEEE Trans. Power Sys.*, vol. 33, no. 1, pp. 116-130, Jan. 2018.

[30] Knut Rapp, "Nonlinear estimation and control in the iron ore pelletizing process: An application and analysis of the Extended Kalman filter", PhD thesis, Norwegian University of Technology, NTNU, 2004.

[31] Z. Xin, X. Wang, Z. Qin, M. Lu, P. C. Loh and F. Blaabjerg, "An Improved Second-Order Generalized Integrator Based Quadrature Signal Generator," *IEEE Trans. Power Electron.*, vol. 31, no. 12, pp. 8068-8073, Dec. 2016.

[32] GB/T 19964-2012, "Technical requirements for connecting photovoltaic power station to power system," Dec. 2012.

Vedantham Lakshmi Srinivas (M' 17) was born in East Godavari, India on 30 October 1994. He received his B. Tech. degree in electrical engineering from Indian Institute of Technology (BHU), Varanasi, India in 2015. He is currently enrolled in Ph.D. in the department of electrical engineering at Indian Institute of Technology Delhi, New Delhi, India. His research interests include renewable energy, energy storage systems, adaptive and learning control, power system dynamics and power electronic converters.

Bhim Singh (SM'99, F'10) was born in Rahamapur, Bijnor (UP), India, in 1956. He received his B.E. (Electrical) from University of Roorkee, India, in 1977 and his M. Tech. (Power Apparatus & Systems) and Ph.D. from the IIT Delhi, India, in 1979 and 1983, respectively. In 1983, he joined the Department of Electrical Engineering, University of Roorkee (Now IIT Roorkee), as a Lecturer. He became a Reader there in 1988. In December 1990, he joined the Department of Electrical Engineering, IIT Delhi, India, as an Assistant Professor, where he has become an Associate Professor in 1994 and a Professor in 1997. He has been Head of the Department of Electrical Engineering at IIT Delhi from July 2014 to August 2016. Presently, he is Dean, Academics at IIT Delhi. He authored the book Power Quality—Problems and Mitigation Techniques (Wiley, 2015).

His areas of research interest include PV grid interface systems, microgrids, power quality, PV water pumping systems, power electronics, electrical machines, drives, FACTS and HVDC systems. Prof. Singh has guided 74 Ph.D. dissertations, 166 M.E./ M.Tech./M.S.(R) thesis. Prof. Singh has more than 37 patents. He has executed more than seventy five sponsored and consultancy projects.

Dr. Sukumar Mishra is a Professor in the Department of Electrical Engineering at the Indian Institute of Technology Delhi. His interest lies in the field of Power Systems, Power Quality Studies, and Renewable Energy. He has published over 100 research articles (including papers in international journals, conferences and book chapters). He is currently holding the position of Vice Chair of Intelligent System Subcommittee of Power and Energy society of IEEE. He is a recipient of the INSA medal for young scientist, the INAE young engineer award, and the INAE silver jubilee young engineer award. He is also a Fellow of IET (UK), NASI (India), INAE (India) and IETE (India). He is actively involved in academic and industrial collaboration for research and development. He is working as the NTPC Chair professor and has previously worked as the Power Grid Chair professor. He is also serving as an Independent Director of the Cross Border Power Transmission Company Ltd. and Industry Academic Distinguish Professor. He has handled many research projects and industrial consultancies.